Open Access Articles

Model Predictive Control of a Nonlinear 2-Body Point Absorber Wave Energy Converter With Estimated State Feedback

The Faculty of Oregon State University has made this article openly available.
Please share how this access benefits you. Your story matters.

Citation	Amann, K. U., Magaña, M. E., & Sawodny, O. (2015). Model Predictive Control of a Nonlinear 2-Body Point Absorber Wave Energy Converter With Estimated State Feedback. [Article in Press]. IEEE Transactions on Sustainable Energy. doi:10.1109/TSTE.2014.2372059
DOI	10.1109/TSTE.2014.2372059
Publisher	IEEE - Institute of Electrical and Electronics Engineers
Version	Accepted Manuscript
Terms of Use	http://cdss.library.oregonstate.edu/sa-termsofuse

Model Predictive Control of a Non-linear 2-Body Point Absorber Wave Energy Converter with Estimated State Feedback

Kai Uwe Amann, Mario E. Magaña, *Senior Member, IEEE* and Oliver Sawodny

***Abstract*—Ocean wave energy has the potential to significantly contribute to sustainable power generation in coastal regions. Much of the research effort has gone into developing time domain state space models of point absorber wave energy converters (WECs) and subsequently into model-based optimal control to efficiently harvest the maximum possible amount of energy. The resulting controllers require knowledge of the states of the WEC in order to achieve the design goals. The purpose of this paper is to design and apply an extended Kalman filter based estimation algorithm to a non-linear two-body WEC model and to evaluate its performance in conjunction with a model predictive controller (MPC) which maximizes energy yield while satisfying operational constraints.**

***Index Terms*—Model predictive control, non-linear point absorber, wave energy converters, Kalman filter**

I. Introduction

THE energy contained in ocean surface waves is wind energy collected over a vast area of the ocean's surface and transported to the shorelines in the concentrated form of gravitational waves. Ongoing efforts as in [1], [2] are made in order to determine suitable methods to find locations where the harvest of this energy is profitable and technically feasible. These demands narrow the list of suitable locations down to mostly exposed west coast regions in the Atlantic and Pacific oceans where high energy density combined with continuity throughout the year and especially during the winter months is prevalent. In order to exploit this energy source and convert it into useful electricity, many different WEC designs like the one presented in [3] have been proposed and evaluated [4], [5] in recent years, one class of devices being the point absorbers. Their dimensions are small compared to the ocean wave lengths they are designed to respond to, making them easier to handle. Usually, point absorbers work best when in resonance with the incoming waves. As a result of the unpredictable nature of ocean waves and their large frequency and amplitude spectrum, active control is needed to maximize power extraction and at the same time provide a certain degree of survivability in harsh sea states. A common type of point absorbers which are also examined in [6], are heaving buoy WECs. They are excited by the heave motion of waves at a fixed location to generate electrical power. Usually these devices feature a type of floating body, the float, that follows the surface movement of the wave. Most devices of this type have a second body, the spar, that is more inert than the float so that a relative motion between the two bodies can be used to generate electricity. The second body is often much heavier than the float and generates a lot of drag in lower, calmer water activity. Additionally it is moored to the sea bed to further inhibit its motion and to keep it on position.

In order to maximize wave energy conversion, optimal model predictive control (MPC) has been applied to point absorber WECs [7], [8], [9], [11], and [12]. In each of these cases, various performance criteria and system constraints have been used to optimise wave energy conversion of a single device. In [11] the performance criterion or cost function is the maximum energy absorption with constraints on the heave motion and the machinery force. In [11], Hals et al also present a two-stage optimisation problem for the regular sea state. Moreover, they propose an MPC algorithm for irregular sea states using real-time prediction of the wave motion horizon. Abraham and Kerrigan [12] investigate a general optimal active control problem for a heaving point absorber whose objective is to maximise the energy extracted from ocean waves, subject to control forces constraints. The hallmark of this paper is that it applies a projected gradient method, which is globally convergent to stationary points using a small number of iterations, to obtain the optimal solution. The works presented in [11] and [12] deal with one-body models and do not consider mooring forces. Moreover, their MPC approaches utilise an available optimal velocity trajectory which can be calculated for one-body WECs. In [8] and [9] a special formulation of the optimal MPC problem which allows the application of MPC without a reference trajectory is applied to maximise the energy extracted from ocean waves subject to machinery constraints of a two-body heaving WEC.

These advanced control algorithms require the knowledge of all states of the modeled WEC and mooring system to operate as intended. As it is often impractical or expensive to measure all states, a state estimation algorithm based on the Kalman filter is proposed in this paper to reduce the amount of required measurements. Additionally, the estimator should be able to handle noisy input signals and noisy plant measurements from cheap sensors which also motivates the use of a Kalman filter. In this paper we propose an extended Kalman filter estimator that yields good performance when the statistical characteristics of the noise process are known and the WEC and

nonlinear mooring system model fit well.

The paper is organized as follows: Section 2 mathematically describes the two-body WEC and the mooring herein considered. Section 3 is mostly devoted to the description of the extended Kalman filter state estimator and details the identification of the filter parameters. In section 4, the WEC system performance is evaluated with the estimator in the MPC control loop. In section 5, the results are summed up and conclusions are drawn.

II. WEC and Mooring Dynamical Model

In this work we consider the generic two-body heaving WEC point absorber shown in Fig. 1. To convert the linear heaving motion into electrical energy, a direct linear generator as described in [13] is used as the power take off system (PTO). The float contains strong permanent magnets which induce a current in a coil inside the spar. Two benefits of this design are the need for only two major movable mechanical parts and the possibility to reverse the generator, using it as an actuator to control the motion of the WEC. The force exercised by the generator will be called F_{PTO} in the following. Other PTO principles are also possible and an overview is presented in [14]. The methods herein presented are independent of the PTO design.

The model of the WEC is based on [15], [16] and consists of the equations of motion for the two moving parts, the float and the spar. The state vector $\mathbf{x} = [z \quad \dot{z} \quad x \quad \dot{x}]$ is composed of the the positions and the velocities of the two bodies as depicted in Fig. 1. To prevent the spar from drifting off its position and to restrict its vertical movement, the WEC is moored to the sea bed. In addition

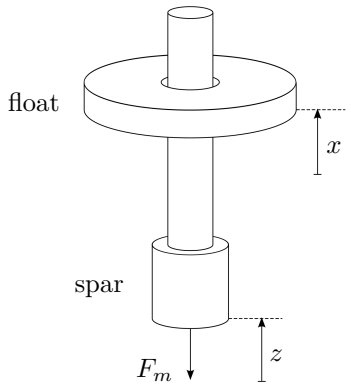

Figure 1: Schematic of the L10 WEC illustrating the displacement variables x and z and the mooring force F_m.

to the already described generator force, the input vector of the model also contains the wave excitation forces F_{e_1} and F_{e_2}, i.e..

$$\underline{u} = (F_{PTO} \; F_{e_1} \; F_{e_2})^T \tag{1}$$

The latter two forces that act on the two bodies are caused by incoming waves. They are difficult to measure directly and thus are calculated from the more easily measurable wave height using a depth dependent filter. The wave height could, for example, be measured by a measuring buoy with appropriate sensors in front of the WEC or be estimated using a stochastic predictor [21].

A. 8-Cable Experimental Mooring

There are many mooring configurations to keep a WEC or group of them from drifting on the ocean surface. Some practical setups that introduce strong nonlinearities might be used to reduce costs or facilitate deployment. In this paper we use a mooring setup suggested by [17] to attach the two-body WEC to a surrounding fixed structure. The device is anchored to the test bed sides by eight identical cables arranged in two crosses at different heights as illustrated in Fig. 2. In [9] this setup is also used to develop a nonlinear MPC which would benefit from a suitable state estimator. The resulting nonlinear mooring force law

$$F_m = 8K_{nl}x\left(1 - \frac{L_{nl}}{\sqrt{L_{nl}^2 + x^2}}\right) \tag{2}$$

with the spring rate K_{nl} as defined in Tab. I does not yield globally acceptable results when linearized

$$F_{m,lin} = -K_m x \tag{3}$$

around a single operating point. This becomes clear when considering the linearization attempt setting K_m to 100,000 $^{\mathrm{N}}/_{\mathrm{m}}$ in Fig. 3. For displacements up to 0.3 m the linearization fits well. For larger displacements the deviation from the actual mooring force grows rapidly. This behavior was also confirmed in [9], where this value for K_m was proposed for medium wave climates. If a reasonable linearization is not possible for one of these setups, the nonlinearity has to be integrated into the plant model, enforcing the use of a nonlinear state estimation algorithm.

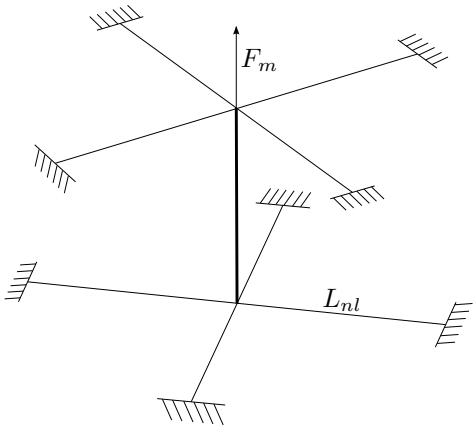

Figure 2: 8-cable mooring configuration with cable length L_{nl} and mooring force F_m.

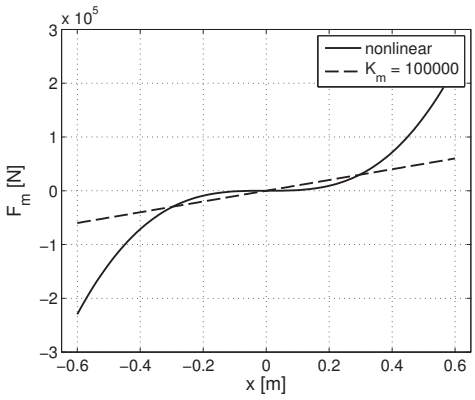

Figure 3: Nonlinear 8-cable mooring force compared to the linearized mooring force with $K_m := 100,000\,\mathrm{N/m}$.

B. WEC/Mooring System State Model

Let us now describe the state space model of the WEC/mooring system that will be used to design the estimation algorithm. The details of the derivation of the state space representation can be found in [8]. Only the final model will be presented here. Let the state vector be described by

$$\underline{x} = (z\ \dot{z}\ x\ \dot{x}\ )^T = (x_1\ x_2\ x_3\ x_4)^T \tag{4}$$

Isolating the nonlinear terms of the model into the vector $l(\underline{x})$, the nonlinear model for the 8-cable experimental mooring can similarly be written as

$$\begin{aligned}\dot{\underline{x}} &= \underline{f}(\underline{x},\underline{u}) \\ &= A_{nl}\underline{x} + l(\underline{x}) + B\underline{u} \\ y &= C\underline{x}\end{aligned} \tag{5}$$

where

$$A_{nl} = \begin{pmatrix} 0 & 1 & 0 & 0 \\ -\frac{k_1}{m_{e_1}} & -\frac{b_1}{m_{e_1}} & 0 & \frac{A_{12}b_2}{m_{e_1}m_{e_{22}}} \\ 0 & 0 & 0 & 1 \\ \frac{A_{21}K_m}{m_{e_2}m_{e_{11}}} & \frac{A_{21}b_1}{m_{e_2}m_{e_{11}}} & 0 & -\frac{b_2}{m_{e_2}} \end{pmatrix} \tag{6}$$

$$l(x) = \begin{pmatrix} 0 \\ -\frac{8A_{12}K_{nl}}{m_{e_1}m_{e_{22}}} \\ 0 \\ -\frac{8K_{nl}}{m_{e_2}} \end{pmatrix} \left(1 - \frac{L_{nl}}{\sqrt{L_{nl}^2 + x_3^2}}\right) x_3 \tag{7}$$

$$B = (B_{PTO}\ B_1\ B_2) \tag{8}$$

$$C = \begin{pmatrix} -1 & 0 & 1 & 0 \end{pmatrix} \tag{9}$$

where

$$B_{PTO} = \begin{pmatrix} 0 \\ \frac{1}{m_{e_1}} + \frac{A_{12}}{m_{e_1}m_{e_{22}}} \\ 0 \\ -\frac{1}{m_{e_2}} - \frac{A_{21}}{m_{e_2}m_{e_{11}}} \end{pmatrix} \tag{10}$$

$$B_1 = \begin{pmatrix} 0 \\ \frac{1}{m_{e_1}} \\ 0 \\ -\frac{A_{21}}{m_{e_2}m_{e_{11}}} \end{pmatrix} \tag{11}$$

$$B_2 = \begin{pmatrix} 0 \\ -\frac{A_{12}}{m_{e_1}m_{e_{22}}} \\ 0 \\ \frac{1}{m_{e_2}} \end{pmatrix} \tag{12}$$

$$m_{e_1} = m_1 + A_{11} - \frac{A_{12}A_{21}}{m_{e_{22}}} \tag{13}$$

$$m_{e_2} = m_2 + A_{22} - \frac{A_{21}A_{12}}{m_{e_{11}}} \tag{14}$$

$$m_{e_{ii}} = m_i + A_{ii}, i = 1, 2.$$

A_{ii} is the hydrodynamic added mass and b_i is the damping that the sea water exercises on the moving WEC parts. The radiation forces, that are the result of convolution terms in the model, are negligibly small and can be excluded for the given device. If necessary, a linear approximation can be included without changing the model structure. B_{PTO}, B_1, and B_2 are the PTO and the excitation forces input distribution matrices, respectively. The input vector is rewritten as

$$\underline{u} = (F_{PTO}\ F_{e_1}\ F_{e_2})^T = (u\ v\ w)^T \tag{15}$$

for a more uniform appearance of the equations. C is the output distribution matrix that describes the relative position. In this work we assume that a sensor which is able to measure the relative position of the float towards the spar is installed on the WEC. The sensor signal is subject to measurement noise.

III. Kalman Filter Estimator

A. Extended Kalman Filter

The main drawback when using a linear Kalman filter estimator on the nonlinear model of the WEC is the fast deviation of the linearized mooring force from the actual one over the occurring range of plant states. As a popular instrument for estimating states of noisy systems, various extensions and modifications of the original Kalman filter exist. One of the most widespread modifications is the extended Kalman [18], which is effective when the nonlinear terms are smooth, slow changing with respect to the discretization time step and not subject to time delays. All these limitations apply to the nonlinear WEC model so the extended Kalman filter is a logical candidate to address the linearization problem in this case. One of the reasons why this type of estimator is so popular in practical applications is its similarity with the linear Kalman filter. It simply linearizes the nonlinear plant model at the most recent state estimation prior to applying a linear Kalman filter. The filter itself is still a linear Kalman filter with a state dependent linearization constant and therefore a state dependent system matrix. The proven optimality of the linear Kalman filter when applied to a linear plant model is no longer verifiable when linearizing a nonlinear model around the current state. The estimation quality will therefore be assessed by simulation results in this work.

1) Discretization of the Nonlinear Model: To make the nonlinear plant model usable by a discrete estimator algorithm, it has to be discretized first. As shown in [18] and [19], a common approach is to develop the model using a Taylor series around the step between the current time and the next time step and derive a formulation for the system state at the next discrete time step based on the current state. For many model types the series can then be truncated after the first order term using the already known derivations of the differential equation system. This method is the same as the Euler forward integration scheme and is suited for linear or near linear systems using small time steps compared to the fastest system dynamics. In this case, however, the nonlinearities are of a kind that are not approximated well by their first derivative and reducing the time steps into the millisecond range does not yield a better performance. To discretize the system the truncated Taylor series can be extended to higher order terms. The nonlinearity in this case requires at least a second order approach to deliver satisfactory results. This was also noticed in [20], leading to a second order approach for the nonlinear MPC as well. Starting with the general system representation as in (5),

$$\dot{\underline{x}} = \mathbf{A}\underline{x} + \mathbf{l}(\underline{x}) + \mathbf{B}\underline{u}, \tag{16}$$

a second order Taylor series approach is made as suggested in [19], i.e.

$$\underline{x}(t+\Delta t) = \underline{x}(t) + \Delta t \frac{\partial}{\partial t}\underline{x}(t) + \frac{(\Delta t)^2}{2}\frac{\partial^2}{\partial t^2}\underline{x}(t) + \mathcal{O}(\Delta t^3). \tag{17}$$

Let Δt be the fixed discretization step size h and

$$\underline{x}_k = \underline{x}(kh) \tag{18}$$

$$\dot{\underline{x}}_k = \left.\frac{\partial}{\partial t}\underline{x}(t)\right|_{t=kh} \tag{19}$$

$$\underline{u}_k = \underline{u}(kh) \tag{20}$$

be the values of $\underline{x}(t)$, $\dot{\underline{x}}(t)$ and $\underline{u}(t)$ at the discrete time steps kh, the second order Taylor series approximation for the discrete system can be formulated as

$$\underline{x}_{k+1} = \underline{f}_d(\underline{x}_k, \underline{u}_k) = \underline{x}_k + h\dot{\underline{x}}_k + \frac{h^2}{2}\ddot{\underline{x}}_k + \mathcal{O}(\Delta t^3). \tag{21}$$

The model equation becomes

$$\begin{aligned}
\underline{x}_{k+1} = {} & \underbrace{\left(I + h\mathbf{A} + \frac{h^2}{2}\mathbf{A}^2\right)}_{\mathbf{A}_{d1}}\underline{x}_k + \underbrace{\left(h\mathbf{I} + \frac{h^2}{2}\mathbf{A}\right)}_{\mathbf{A}_{d2}}\mathbf{l}(\underline{x}_k) \\
& + \frac{h^2}{2}\mathbf{l}'(\underline{x}_k)\mathbf{A}\underline{x}_k + \frac{h^2}{2}\mathbf{l}'(\underline{x}_k)\mathbf{l}(\underline{x}_k) \\
& + \underbrace{\left(h\mathbf{B} + \frac{h^2}{2}\mathbf{A}\mathbf{B}\right)}_{\mathbf{B}_d}\underline{u}_k + \frac{h^2}{2}\mathbf{l}'(\underline{x}_k)\mathbf{B}\underline{u}_k \\
& + \frac{h^2}{2}\mathbf{B}\dot{\underline{u}}_k \\
= {} & \mathbf{A}_{d1}\underline{x}_k + \mathbf{A}_{d2}\mathbf{l}(\underline{x}_k) + \frac{h^2}{2}\mathbf{l}'(\underline{x}_k)\mathbf{A}\underline{x}_k \\
& + \frac{h^2}{2}\mathbf{l}'(\underline{x}_k)\mathbf{l}(\underline{x}_k) + \mathbf{B}_d\underline{u}_k + \frac{h^2}{2}\mathbf{l}'(\underline{x}_k)\mathbf{B}\underline{u}_k.
\end{aligned} \tag{22}$$

where

$$\mathbf{l}'(x_3) = \begin{pmatrix} 0 & 0 & 0 & 0 \\ 0 & 0 & -\frac{8A_{12}K_{nl}}{m_{e_1}m_{e_2}{}^2}\left(1 - \frac{L_{nl}^3}{(L_{nl}^2+x_3^2)^{1.5}}\right) & 0 \\ 0 & 0 & 0 & 0 \\ 0 & 0 & -\frac{8K_{nl}}{m_{e_2}}\left(1 - \frac{L_{nl}^3}{(L_{nl}^2+x_3^2)^{1.5}}\right) & 0 \end{pmatrix} \tag{23}$$

is the Jacobian matrix of $\mathbf{l}(\underline{x})$. The last version (22) is compatible with the notation used in [20] and the simulation setup.

2) Discrete-time Extended Kalman Filter: Now that a discrete nonlinear plant model is available, the filter algorithm itself will be modified appropriately. According to [18], the basic idea is to linearize this model around the last state estimation at every discrete time step. Using a linear model for the filter algorithm and small time steps, the deviations from the nonlinear model are held very small. Basically, it is a linearization around the best available trajectory without future knowledge of the trajectory itself. The effect on the algorithm itself is that the system matrix $\mathbf{F}$ is no longer constant but changes at each time step and is hence indexed with the time step of the last estimated system state as $\mathbf{F}_{k-1}$.

If the process or measurement noise are subject to nonlinear transformations before they are incorporated into the system, special care needs to be taken when linearizing the system equations for use with the extended Kalman filter. Because the covariance matrix P of a stochastic vector $\underline{x}$ with a mean $\bar{\underline{x}}$ is

$$P = E\left[(\underline{x} - \bar{\underline{x}})(\underline{x} - \bar{\underline{x}})^T\right], \tag{24}$$

it is not sufficient to just transform the covariance by subjecting P to the transformation $f(\underline{x})$. Furthermore, a nonlinear transformation of the white noise process results in non white noise and distorted noise power distributions. In the case of this model, the nonlinearity is a function of the system states only so that these considerations do not apply.

Starting with the nonlinear discrete-time plant model (22) a linearized discrete model

$$\underline{x}_{k+1} = \mathbf{F}_k\underline{x}_k + \mathbf{G}_k\underline{u}_k + \underline{\omega}_k \tag{25}$$

$$\underline{y}_k = \mathbf{C}\underline{x}_k + \underline{v}_k \tag{26}$$

is calculated at every time step. $\underline{\omega}_k$ and $\underline{v}_k$ are the process and measurement noise vectors, respectively. In this special case of a relatively simple nonlinear term which is only dependent on the state x_3, the system matrix

$$\mathbf{F}_k \cong \mathbf{A}_{d1} + \mathbf{A}_{d2}\mathbf{l}'(\hat{\underline{x}}_{k-1}^+) + \frac{h^2}{2}\left.(\mathbf{l}'(\underline{x})\mathbf{A}\underline{x})'\right|_{\hat{\underline{x}}_{k-1}^+} \tag{27}$$

contains only a few terms with $\hat{\underline{x}}_k^+$ being the state measurement update. When a different model is used that contains more nonlinear terms and dependencies on multiple states, the formal description of the second derivative $l''(\underline{x})$ will be a 3 dimensional matrix which then requires tensor calculus to be applied to the expressions. In this simple case it is still feasible and less complex to calculate the

derivatives by hand and intuition rather than resorting to a closed form description of all the terms. The only possibly troublesome term

$$\left(\mathbf{l}'(\underline{x})\mathbf{A}\underline{x}\right)'\Big|_{\underline{\hat{x}}^+_{k-1}} = \begin{bmatrix} 0 & 0 & 0 & 0 \\ 0 & 0 & l_2''(\hat{x}^+_{3,k-1})\hat{x}^+_{4,k-1} & l_2'(\hat{x}^+_{3,k-1}) \\ 0 & 0 & 0 & 0 \\ 0 & 0 & l_4''(\hat{x}^+_{3,k-1})\hat{x}^+_{4,k-1} & l_4'(\hat{x}^+_{3,k-1}) \end{bmatrix}$$

yields a very manageable result. In the end, only four derivative terms of the form

$$l_i''(x_3) = \frac{\partial^2 l_i(\underline{x})}{\partial x_3^2} \tag{28}$$

are left. Due to the simple structure of the nonlinearity, we obtain

$$\begin{pmatrix} l_1''(x_3) \\ l_2''(x_3) \\ l_3''(x_3) \\ l_4''(x_3) \end{pmatrix} = \begin{pmatrix} 0 \\ -\frac{8A_{12}K_{nl}}{m_{e_1}(m_2+A_{22})} \\ 0 \\ -\frac{8K_{nl}}{m_{e_2}} \end{pmatrix} \frac{3L_{nl}^3}{\left(L_{nl}^2+x_3^2\right)^{2.5}} x_3. \tag{29}$$

The input distribution matrix of the discrete equivalent WEC/mooring system is now described by

$$\mathbf{G}_k = \mathbf{B}_d + \frac{h^2}{2}\mathbf{l}'(\underline{\hat{x}}^+_{k-1})\mathbf{B}. \tag{30}$$

Moreover, $\underline{\omega}_k = G_k\xi_k$, where ξ_k is the process noise associated with the excitation forces F_{e_1} and F_{e_2}. The discrete linearized plant model can thus be derived without resorting to a $4\times4\times4$ tensor, describing the multivariate counterpart of the univariate Hessian Matrix. After calculating the step-specific discrete plant linearization, the rest of the Kalman filter algorithm remains the same as the linear implementation, namely,

$$\underline{\hat{x}}^-_k = \mathbf{F}_{k-1}\underline{\hat{x}}^+_{k-1} + \mathbf{G}_{k-1}\underline{u}_{k-1} \tag{31}$$
$$\mathbf{P}^-_k = \mathbf{F}_{k-1}\mathbf{P}^+_{k-1}\mathbf{F}^T_{k-1} + \mathbf{Q}_{k-1} \tag{32}$$
$$\mathbf{K}_k = \mathbf{P}^-_k\mathbf{C}^T\left(\mathbf{C}\mathbf{P}^-_k\mathbf{C}^T + \mathbf{R}_k\right)^{-1} \tag{33}$$
$$\underline{\hat{x}}^+_k = \underline{\hat{x}}^-_k + \mathbf{K}_k\left(y_k - \mathbf{C}\underline{\hat{x}}^-_k\right) \tag{34}$$
$$\mathbf{P}^+_k = \left(\mathbf{I}-\mathbf{K}_k\mathbf{C}\right)\mathbf{P}^-_k\left(\mathbf{I}-\mathbf{K}_k\mathbf{C}\right)^T + \mathbf{K}_k\mathbf{R}_k\mathbf{K}^T_k \tag{35}$$

where $\underline{\hat{x}}^-_k$ is the state time update, Q_k is the input noise covariance matrix, R_k is the measurement noise covariance matrix, P^-_k is the a priori error covariance matrix, P^+_k is the a posteriori error covariance matrix and K_k is the feedback gain matrix that weighs the error between the actual system output and the a priori estimated output.

This filter does not guarantee optimality any more, not even if the corresponding requirements concerning the noise process and an exact plant model are satisfied. However, it is the most common nonlinear state estimation algorithm in use, mostly because of its similarity to the well known Kalman filter. As soon as the discretized and linearized model are known, the implementation in software is straight forward.

Table I: System parameters

Parameter	Value
m_1	2625.3 kg
m_2	2650.4 kg
A_{11}	8866.7 kg
A_{22}	361.99 kg
A_{12}	361.99 kg
A_{21}	361.99 kg
b_1	5000 N/(m/s)
b_2	50000 N/(m/s)
k_1	96743 N/m
K_m	100000 N/m
K_{nl}	840000 N/m
L_{nl}	1.7 m

IV. Simulation Results

Uncontrolled (open-loop) and controlled (closed-loop) WEC tracking performance of the Kalman filter estimator is quantified via computer simulation. Controlled WEC power generation performance will be measured using the Kalman filter estimator in the control loop.

A time series from the National Data Buoy Center (NDBC) Umpqua buoy 46229 which is deployed off the coast of Oregon north of Reedsport [22] is used to calculate the excitation forces F_{e_1} and F_{e_2}. The wave is characterized by a significant height of 1.97 m, energy period of 6.39 s, dominant period of 6.13 s, and a power of 12.1 kW/m of crest length.

A. Uncontrolled WEC Tracking performance with Measurement Noise

For comparison purposes, we also test a linear Kalman filter designed around the linearized version of the nonlinear model (5) on the basis of the linearized mooring force (3) where the spring constant K_m is set to 100,000 N/m as proposed in [9] as a compromise for medium sea states.

Tab. I lists the physical parameters used in the simulations. These parameters are taken from [8], [9] so that the same simulation environment can be used to test the estimation algorithms.

The simulation uses a measurement noise covariance of $R := 0.4\,\mathrm{m}^2$.

At this stage no process noise is added. Tracking performance of both linear and extended Kalman filters is shown in Fig. 4. The position of the float in Fig. 4a is estimated nearly perfectly by both filters. This is due to the fact that the equation for the first state is not directly influenced by the nonlinearity and the continuous correction through the measured plant output ensures good tracking of the actual state. The float speed in Fig. 4b shows some minor deviations in the linear case, though its estimate is still quite good, since the float is only indirectly influenced by the mooring. The spar on the other hand is influenced far more severely by the imprecise mooring linearization. Figures 4c and 4d show deviations of over 40 % of the actual amplitude in the case of the linear filter. Apart

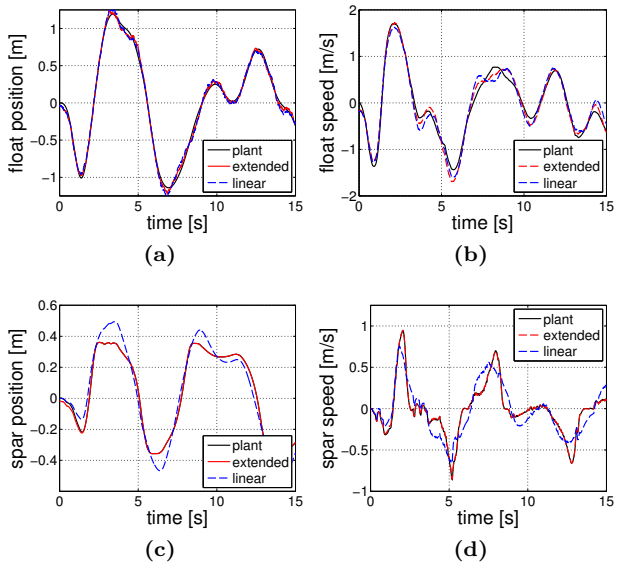

Figure 4: Performance comparison of the extended Kalman filter (extended) with that of the linear Kalman filter (linear) using an uncontrolled nonlinear reference plant model (plant) with measurement noise affecting the filter inputs.

from quantitative deviations of the estimates of the linear Kalman filter, the signal quality of the estimation of the spar speed is very different from the actual signal: The signal peaks of the spar speed in Fig. 4d are smoothed off and reduced by about 25 %. With an MPC in mind that has to obey spar speed constraints, state underestimation will make it impossible for the controller to keep the state within the specified bounds. As a result, the linear Kalman filter is not suitable to adequately estimate the states of this nonlinear plant model. Hence, the nonlinear characteristics of the model have to be incorporated into the estimator design. Figs. 4c and 4d clearly show that the inclusion of the nonlinear model properties into the extended Kalman filter estimator design substantially improves the estimation of the spar states.

To complete the comparison, a practical evaluation of the needed computational effort is made on an Intel Core i7-4810 CPU running an unoptimized Matlab-S-Function implementation of the linear and extended Kalman filter algorithms. The linear filter computes with a mean execution time of 22.9 μs compared to 35.2 μs for the extended implementation. This is an increase of 53 %.

B. Identification of the Covariance Matrices $\mathbf{Q}$ *and* $\mathbf{R}$

When the input and measurement noise covariances are not known beforehand, correlation methods such as the innovation correlation method or covariance matching as suggested in [25] or more recent approaches for autocovariance least squares methods as in [27] or by applying methods based on semidefinite programming and optimal weighting as in [26] should be used.

Assuming a perfect plant model and complete knowledge of the system and measurement noise processes, the Kalman filter would not have tunable parameters. There would only be deterministically identifiable constants, namely the covariances $\mathbf{Q}$ and $\mathbf{R}$ of the system and measurement noise, that need to be included. In most practical cases these parameters and the plant model are not known exactly or may change over time, thus, a certain amount of manual tuning may be needed to improve filter performance.

The covariance $\mathbf{R}$ of the measurement noise can be seen as the measure of trust the filter has of the measured plant output. Increasing these values makes the filter prefer the estimated system output over the measured output in the feedback loop. This behavior can be exploited to compensate for uncertainties in the calculated covariances or to account for noise processes that differ from white Gaussian noise. The penalty for raising the covariances in $\mathbf{R}$ above the actual covariance of the assumed measurement noise is the loss of some optimality.

The model process noise resembles an uncertainty in the plant model and can be used to make the filter more robust against modeling errors to a certain degree. Although process noise is not a good way to model non stochastic model errors, in the case of the WEC it is reasonable to put more trust in the measurements than into the system model as it is not exactly known and may change over time. In principle the Kalman filter is not designed for robustness against modeling errors, so only a small amount of robustness can be achieved by utilizing process noise for this task. A more suitable method would be moving horizon filtering as discussed in [24], but the added processing time and problem complexity make it less suitable for environments with constrained computing power and high demands for cheap and robust embedded hardware.

Process noise can also be used to take input noise into consideration. To identify the entries of the $\mathbf{Q}$ matrix for this case, the influence of input noise on the stochastic plant model has to be analyzed first.

1) Modeling Input Noise: The added input noise is assumed to be zero mean white Gaussian noise, the same characteristics as the already introduced process noise ω and the measurement noise ν. The new input

$$\underline{\tilde{u}} = \underline{u} + \underline{\xi} \tag{36}$$

$$\underline{\xi} \sim \text{Gauss}\left(\underline{0}, \mathbf{Q}_{c,u}\right) \tag{37}$$

consists of the undisturbed measurement $\underline{u}$ and the added measurement noise $\underline{\xi}$ with continuous covariance matrix $\mathbf{Q}_{c,u}$. Inserting the new input into the linear model yields the system equation

$$\dot{\underline{x}} = \mathbf{A}\underline{x} + \mathbf{B}\underline{u} + \mathbf{B}\underline{\xi} + \underline{\omega} \tag{38}$$

$$\underline{\omega} \sim \text{Gauss}\left(\underline{0}, \mathbf{Q}_{c}\right) \tag{39}$$

$$\underline{\xi} \sim \text{Gauss}\left(\underline{0}, \mathbf{Q}_{c,u}\right) \tag{40}$$

containing the propagated input noise $\underline{\xi}$. To regain a formulation that is compatible with the Kalman filter design equations, the measurement noise has to be integrated into

the process noise as a pure zero mean Gaussian process

$$\underline{\omega}_u = \mathbf{B}\underline{\xi}. \tag{41}$$

This is possible because using linear transformations, only the covariances of the noise process change, but not the fundamental white noise property. To design the filter only certain characteristics of the input noise have to be known. These are the mean value and the covariance. The transformations of these characteristics are obtained by inserting the transformed variable into the formula used to calculate the characteristics. The mean value of $\underline{\omega}_u$ is

$$E(\underline{\omega}_u) = E(\mathbf{B}\underline{\xi}) \tag{42}$$

is still zero, whereas its covariance matrix is

$$\begin{aligned}\mathbf{Q}_u &= E(\underline{\omega}_u\underline{\omega}_u^T) && (43)\\ &= E((\mathbf{B}\underline{\xi})(\mathbf{B}\underline{\xi})^T) && (44)\\ &= \mathbf{B}\mathbf{Q}_{c,u}\mathbf{B}^T && (45)\end{aligned}$$

Applying the new input noise process to the discrete plant model,

$$\begin{aligned}\underline{x}_k &= \mathbf{F}\underline{x}_{k-1} + \mathbf{G}\underline{u}_{k-1} - \underline{\omega}_{u,k-1} + \underline{\omega}_{k-1} && (46)\\ \underline{\omega}_k &\sim \text{Gauss}\,(\underline{0}, \mathbf{Q}) && (47)\\ \underline{\omega}_{u_k} &\sim \text{Gauss}\,(\underline{0}, \mathbf{Q}_u) && (48)\\ \mathbf{Q}_{u_k} &\approx \mathbf{Q}_u\Delta t. && (49)\end{aligned}$$

is obtained as the new model with the input noise integrated into the plant's process noise.

Using the known covariances $[0, 10^9\,\text{N}^2, 10^5\,\text{N}^2]$ of the input signals F_{PTO}, F_{e_1} and F_{e_2}, the covariance matrix of the transformed input noise results in

$$\mathbf{Q}_u = \begin{pmatrix} 0 & 0 & 0 & 0 \\ 0 & 7.6296 & 0 & -0.9172 \\ 0 & 0 & 0 & 0 \\ 0 & -0.9172 & 0 & 0.1213 \end{pmatrix} \Delta t. \tag{50}$$

As the input signals affect the states x_2 and x_4, the corresponding process noise for these states is no longer uncorrelated. The off diagonal elements of $\mathbf{Q}_u$, also called cross covariances, represent a correlation between the two process noise terms. The identified covariance matrix can now be used to integrate the input noise into the process noise. But there are still zeros for the diagonal entries of the process noise for the states x_1 and x_3. Even though these states are not affected by input noise, it is still a good idea to add at least a little bit of system noise. No noise at all will lead to numerical problems when evaluating the error covariance matrix $\mathbf{P}$, as it will be stuck at zero values, if they should occur during the operation of the filter. To counter any problems of this kind, the diagonal elements of the process noise covariance matrix $\mathbf{Q}$ will be set to a value about one magnitude below the entries of the input covariance matrix. A value of 0.01 for the diagonal elements has proven to reliably prevent any numerical problems during simulations.

A simulation with these covariances produces close to exact results for the x_3 and x_4 states right away but leaves some room for improvement concerning the estimation of states x_1 and x_2 as can be seen in the detail plots in Fig. 5. Especially the float position is still a bit noisy. This state will be very important for the MPC to fulfill the position constraints which in turn are important mechanical constraints for the survival of the WEC. As a result the covariance for the x_2 process noise is manually tuned to achieve a better compromise regarding the residual noise of x_1. The simulation result after setting $Q_{2,2} := 1$ can also be seen in Fig. 5. By reducing the expected covariance for x_2, the estimates for x_1 are smoother at the cost of a bit more deviation from the exact state x_2.

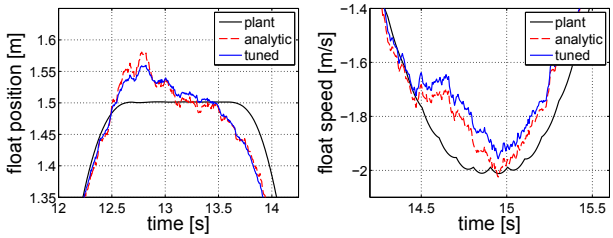

(a) (b)

Figure 5: Detailed view of a performance comparison demonstrating the analytically identified covariances (analytic), the manually tuned covariances (tuned) and the exact internal reference states of the plant (plant).

C. Controlled WEC Performance with Process and Measurement Noise

The extended Kalman filter is now integrated into the feedback loop as shown in Fig. 6 and tested in the presence of both input and measurement noise. This is done to assess WEC system performance under noisy conditions.

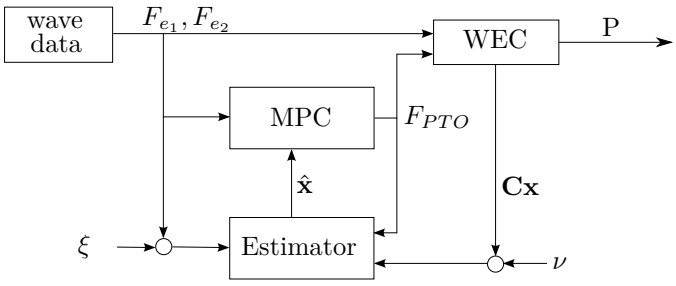

Figure 6: State estimator integrated into the control loop.

The non-linear MPC (NMPC) is implemented using Matlab/SIMULINK. The NMPC uses the solver "fmincon" of Matlab which can handle nonlinear problems with nonlinear constraints. Here, the interior-point method is used as the optimization algorithm of "fmincon".

The objective function is formulated to include one term expressing the generated power and another term presenting the energy use. In general, the generated power for point absorbers is the product of relative velocity and PTO force. Furthermore, the optimization problem

includes slack variables ϵ_p and ϵ_v to add position and velocity slack as in [23] to avoid infeasibilities. Introducing

$$\underline{p} = \begin{bmatrix} \underline{\hat{x}}_1^T & u_0 & \underline{\hat{x}}_2^T & u_1 & \dots & \underline{\hat{x}}_N^T & u_{N-1} & \epsilon_1 & \epsilon_2 \end{bmatrix}^T \quad (51)$$

as the vector of optimization variables, the optimization problem is stated as

$$\min_{\underline{p}} \; J(\underline{p}), \quad (52)$$

$$J(\underline{p}) = \sum_{k=1}^{N} \left[\xi \big(\underline{\hat{x}}_{k,(2)} - \underline{\hat{x}}_{k,(4)} \big) u_{k-1} \; + \gamma \, u_{k-1}^2 \right] + w_p \epsilon_1^2 + w_v \epsilon_2^2, \quad (53)$$

subject to

$$\underline{\hat{x}}_{k+1} = \underline{f}_d(\underline{\hat{x}}_k, u_k, v_k, w_k) \quad (54)$$

$$|\underline{\hat{x}}_{k,(1)} - \underline{\hat{x}}_{k,(3)}| - \epsilon_1 \leq c_p, \qquad k = 1, \dots, N \quad (55)$$

$$|\underline{\hat{x}}_{k,(2)} - \underline{\hat{x}}_{k,(4)}| - \epsilon_2 \leq c_v, \qquad k = 1, \dots, N \quad (56)$$

$$|u_k| \leq c_u, \qquad k = 0, \dots, N-1 \quad (57)$$

$$0 \leq \epsilon_p \leq c_{\epsilon_p}, \qquad 0 \leq \epsilon_v \leq c_{\epsilon_v}, \quad (58)$$

where c_p, c_v and c_u are the relative position, velocity and the generator constraints, respectively. w_p and w_c are the weighting factors that penalize the slack variables, and c_{ϵ_p} and c_{ϵ_v} are their corresponding constraints. $\underline{\hat{x}}_{k,(i)}$ is the estimated discrete state vector component of index i.

The algorithm is implemented using the optimization vector $\underline{p}$ with $5N + 2$ variables. It is straightforward to express the objective function by means of $\underline{p}$. The solver "fmincon" can handle box constraints, linear and nonlinear inequality and equality constraints. The slack variables (58) and the input constraints (57) are considered as box constraints which yield $2N+4$ equations. The position (55) and velocity (56) limits are considered as linear inequality constraints which yield $4N$ equations. Additionally, the system dynamics (54) need to be included as constraints, here as nonlinear equation constraints with $4N$ equations.

According to [21], the wave's motion can be accurately predicted for up to two typical wave periods into the future. Thus, a prediction time of at least 10 s is realistic. However, it should be noted that a large horizon time normally improves the performance, but at the same time, the computational effort increases since the optimization complexity increases. Since the results with a larger horizon time are not significantly better, a horizon time of 3 s is used which normally contains a half wave period and thus, the dominant dynamics. In what follows, $T_{hor} := 3\,\text{s}$ and $\Delta T := 0.1\,\text{s}$. Thus the horizon length is 30 steps.

The simulations and control parameters are shown in Table II.

Fig. 7 shows the results and it is evident that in the case of the spar position the extended Kalman filter keeps the MPC within the bounds whereas the linear Kalman filter exceeds the maximum value by over 25 % as expected, which may result in mechanical damage. Overall, it can be said that the extended Kalman filter performs well

Table II: NMPC/MPC parameter values.

Parameter	Description	Value
Δt	sample time for optimization	0.1 s
T_{hor}	Optimization horizon	3 s
N	Number of values	30
T	Simulation Time	15 s
ξ	Power weighting factor	1
γ	Input weighting factor	0
c_p	Relative position constraint	1 m
c_v	Relative velocity constraint	0.9 m/s
c_u	Generator force constraint	50,000 N
c_{ϵ_p}	Position slack var. constraint	0.1 m
c_{ϵ_v}	Velocity slack var. constraint	1 m/s
w_p	Position slack weight	10^8
w_v	Velocity slack weight	10^6

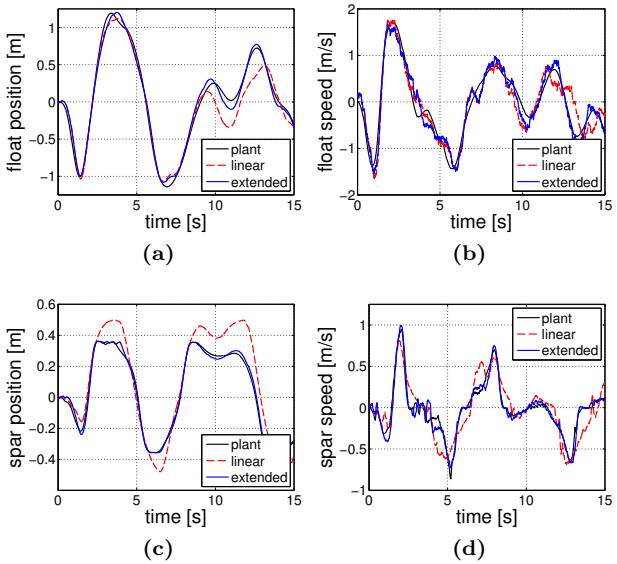

Figure 7: Performance of the extended Kalman filter (extended) compared to the linear Kalman filter (linear) integrated into the MPC feedback loop on the nonlinear plant model with measurement and input noise. The actual plant states (plant) of a simulation without estimators in the loop is given as a reference.

enough to achieve a comparable performance to measuring all states directly.

Fig. 8 shows that the control signal F_{PTO} of the extended Kalman filter estimator is very close to the control signal of an MPC directly using the plant states. The linear Kalman filter cannot track the plant states after the saturation event at 9 seconds and provides the MPC with wrong measurements leading to a very different input force trajectory.

The WEC output power is now analyzed for the nonlinear model. The simulation results in Fig. 9 show that for larger wave heights both estimators are reasonably close to the power output trajectory of the controller directly using the actual plant states. At lower power outputs the linear Kalman filter's inability to estimate the states as precisely

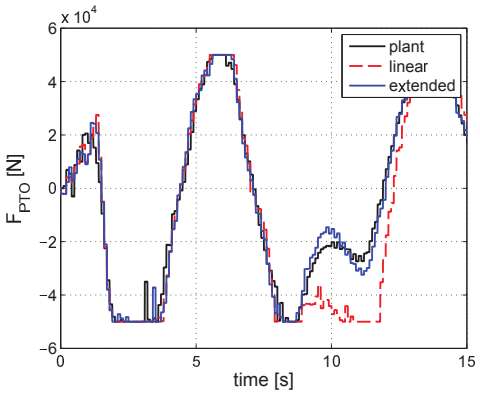

Figure 8: MPC output F_{PTO} comparison between the in-loop linear (linear) and extended Kalman filters (extended) and actual WEC system states (plant). WEC system is subjected to both measurement and input process noise.

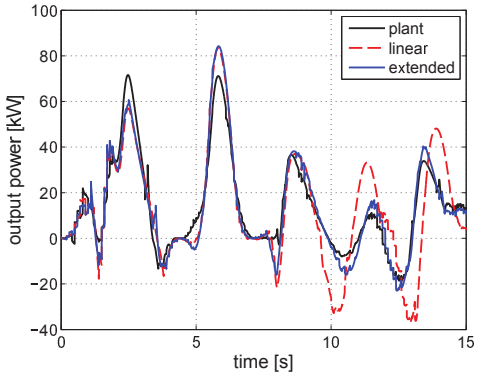

Figure 9: Output power comparison between systems which use the actual plant states (plant) and states estimated by either a linear Kalman filter (linear) or an extended Kalman filter (extended). The WEC system is subjected to both measurement and input process noise.

as the extended Kalman filter leads to sub optimal power extraction. This can be verified by comparing the average output power. With the actual state values, the WEC extracts a mean power of 6.081 kW over a time interval of 25 s. The linear Kalman filter reduces this to 5.461 kW and the extended Kalman filter to 5.926 kW. This corresponds to efficiency factors of 89.8 % for the linear and 97.4 % for the extended filter. Thus, the power output benefits significantly from the consideration of the nonlinear mooring effects.

V. Conclusion

As expected, the results showed that the linear Kalman filter estimator cannot deliver precise state estimates as the extended Kalman filter when applying it to a WEC with nonlinear mooring and in the presence of noise. The simulations with the extended Kalman filter integrated into the control loop showed promising results and very small losses in generated average power. This advantage comes at an increase in computational effort of 53 % for this use case, so if a device is capable of running the linear filter, the extended Kalman filter should also be possible to run in real time.

It was shown that it is possible to reconstruct the system states by only using the relative position between the two bodies and the wave height data. This holds for both linear and nonlinear mooring forces and the considered MPC. From a computational point of view, the proposed filters are easy to implement as long as basic matrix operations are possible on the targeted platform. Since the system is only of fourth order, any modern embedded hardware should be able to run the algorithms in real time.

The mathematical model of the WEC herein used was assumed to be a faithful representation of its dynamics. However, a laboratory verification still needs to be done. Future research has to address WEC modeling errors and parameter variations. Also, an H_∞ estimator might be a possible alternative to the Kalman filter, if the latter cannot be made robust enough.

References

[1] Oezger M., Altunkaynak A., and Sen Z., "Statistical investigation of expected wave energy and its reliability," *Energy Conversion and Management*, vol. 45, pp. 2173–2185, 2004.

[2] Carballo R. and Iglesias G., "A methodology to determine the power performance of wave energy converters at a particular coastal location," *Energy Conversion and Management*, vol. 61, pp. 8–18, 2012.

[3] Bracco G., Giorcelli E., and Mattiazzo G., "A gyroscopic mechanism for wave power exploitation," *Mechanism and Machine Theory*, vol. 46, pp. 1411-1424, 2011.

[4] Oskamp J. A. and Ozkan-Haller, H. T., "Power calculations for a passively tuned point absorber wave energy converter on the oregon coast," *Renewable Energy*, vol. 45, pp. 72–77, 2012.

[5] Babarit A., Hals J., Muliawan M., Kurniawan A., Moan T., and Krokstad J., "Numerical benchmarking study of a selection of wave energy converters," *Renewable Energy*, vol. 41, pp. 44–63, 2012.

[6] Al-Habaibeh A., Su D., McCague J., and Knight A., "An innovative approach for energy generation from waves," *Energy Conversion and Management*, vol. 51, pp. 1664–1668, 2010.

[7] Brekken, T.K.A., "On Model Predictive Control for a point absorber Wave Energy Converter," in *2011 IEEE PowerTech, Trondheim, Norway*, pp. 1–8, june, 2011.

[8] M. Richter, M. E. Magaña, O. Sawodny, and T. K. A. Brekken, "Power optimization of a point absorber wave energy converter by means of linear model predictive control," *IET Renewable Power Generation*, vol. 8, no. 2, pp. 203-215, 2014.

[9] M. Richter, M. E. Magaña, O. Sawodny, and T. K. A. Brekken, "Nonlinear model predictive control of a point absorber wave energy converter," *IEEE Transactions on Sustainable Energy*, vol. 4, no. 1, pp. 118–126, Jan. 2013.

[10] J. Falnes, *Ocean Waves and Oscillating Systems, Linear Interaction Including Wave-Energy Extraction*. Cambridge University Press, 2002.

[11] J. Hals, J. Falnes, and T. Moan, "Constrained optimal control of a heaving buoy wave-energy converter," *Journal of Offshore Mechanics and Artic Engineering*, vol. 133, pp. 1–15, Feb. 2011.

[12] E. Abraham and E. C. Kerrigan, "Optimal active control and optimization of a wave energy converter," *IEEE Transactions on Sustainable Energy*, vol. 4, no. 2, pp. 324–332, April 2013.

[13] Elwood, D, Schacher, A, Rhinefrank, K, Prudell, J, Yim, S and Amon, E, "Numerical modelling and ocean testing of a direct-drive wave energy device utilizing a permanent magnet linear generator for power take-off," in *Proceedings of 28th International Conference on Ocean Offshore Arctic Engineering, ASME, Honolulu, Hawaii*, 2009.

[14] A. F. O. FalcÃčo, "Wave energy utilization: A review of the technologies," *Renewable and Sustainable Energy Reviews*, vol. 14, No. 3, pp. 899–918, 2010.

[15] Ruehl, K. "Time-Domain Modeling of Heaving Point Absorber Wave Energy Converters, Including Power Take-Off and Mooring," MS Thesis, Mechanical Engineering, Oregon State University, 2011.
[16] H. Eidsmoen, "Simulation of a slack-moored heaving-buoy wave-energy converter with phase control," PhD thesis, Norwegian University of Science and Technology, Trondheim, Norway, 1996.
[17] Y. Li and Y.H. Yu, "Preliminary results of a RANS simulation for a foating point absorber wave energy system under extreme wave condition," *30th International Conference on Ocean, Offshore, and Artic Engineering*, Rotterdam, The Netherlands, June 19-24, 2011.
[18] Simon, D., *Optimal State Estimation: Kalman, H [infinity] and Nonlinear Approaches*, Wiley-Interscience, 2006.
[19] Vidyasagar, M., *Nonlinear systems analysis*, Prentice-Hall, 1978.
[20] Markus Richter, *Different Model Predictive Control Approaches for Controlling Point Absorber Wave Energy Converters*, MS Thesis, Institute for System Dynamics, Stuttgart, Germany, 2011.
[21] Fusco, F. and Ringwood, J.V., "Short-Term Wave Forecasting for Real-Time Control of Wave Energy Converters," *IEEE Transactions on Sustainable Energy,*, 2010, Vol. 1, No. 2, pp. 99–106, July 2010.
[22] National Data Buoy Center, http://www.ndbc.noaa.gov/, Sept. 2011.
[23] Richter M., *Different model predictive conrol approaches for controlling point absorber wave energy converters*, MS Thesis, Oregon State University, 2011.
[24] Eric L. Haseltine, James B. Rawlings, *Critical Evaluation of Extended Kalman Filtering and Moving-Horizon Estimation*, Industrial & Engineering Chemistry Research, Vol. 44, No. 8. (29 June 2004), pp. 2451-2460.
[25] Mehra, R.K., *Approaches to adaptive filtering*, Automatic Control, IEEE Transactions on , vol.17, no.5, pp.693,698, Oct 1972
[26] Brian J. Odelson, Murali R. Rajamani, James B. Rawlings, *A new autocovariance least-squares method for estimating noise covariances*, Automatica, Volume 42, Issue 2, February 2006, Pages 303-308
[27] Murali R. Rajamani, James B. Rawlings, *Estimation of the disturbance structure from data using semidefinite programming and optimal weighting*, Automatica, Volume 45, Issue 1, January 2009, Pages 142-148